Korean J. Chem. Eng., 33(2), 514-526 (2016)
DOI: 10.1007/s11814-015-0154-3

pISSN: 0256-1115
eISSN: 1975-7220

Properties of $LiNi_{0.8}Co_{0.1}Mn_{0.1}O_2$ as a high energy cathode material for lithium-ion batteries

Duc-Luong Vu and Jae-won Lee†

Department of Energy of Engineering, Dankook University, Cheoan 330-714, Korea
(*Received 18 March 2015 • accepted 10 July 2015*)

Abstract−Nickel-rich layered materials are prospective cathode materials for use in lithium-ion batteries due to their higher capacity and lower cost relative to $LiCoO_2$. In this work, spherical $Ni_{0.8}Co_{0.1}Mn_{0.1}(OH)_2$ precursors are successfully synthesized through a co-precipitation method. The synthetic conditions of the precursors - including the pH, stirring speed, molar ratio of NH_4OH to transition metals and reaction temperature - are investigated in detail, and their variations have significant effects on the morphology, microstructure and tap-density of the prepared $Ni_{0.8}Co_{0.1}Mn_{0.1}(OH)_2$ precursors. $LiNi_{0.8}Co_{0.1}Mn_{0.1}O_2$ is then prepared from these precursors through a reaction with 5% excess $LiOH\cdot H_2O$ at various temperatures. The crystal structure, morphology and electrochemical properties of the $Ni_{0.8}Co_{0.1}Mn_{0.1}(OH)_2$ precursors and $LiNi_{0.8}Co_{0.1}Mn_{0.1}O_2$ were investigated. In the voltage range from 3.0 to 4.3 V, $LiNi_{0.8}Co_{0.1}Mn_{0.1}O_2$ exhibits an initial discharge capacity of 193.0 mAh g^{-1} at a 0.1 C-rate. The cathode delivers an initial capacity of 170.4 mAh g^{-1} at a 1 C-rate, and it retains 90.4% of its capacity after 100 cycles.

Keywords: Lithium-ion Battery, Cathode Material, $LiNi_{0.8}Co_{0.1}Mn_{0.1}O_2$, Co-precipitation, Electrochemical Properties

INTRODUCTION

Lithium-ion batteries are promising power supplies for use in electric vehicles due to their high energy density and long cycling life relative to other secondary batteries [1-5], and layered lithium transition metal oxides are by far the most extensively used cathode materials for lithium ion batteries [6-8]. However, these suffer from several shortcomings, including a poor structural stability, an inability to extract all lithium ions and the high cost and toxicity of cobalt [9-11]. Therefore it is important to develop alternative cathode materials in order to obtain a higher capacity, improved safety and lower cost. $LiNiO_2$ is one of the most attractive candidate materials that has been suggested so far to meet these requirements because it has been shown to attain a higher reversible capacity with a lower cost than $LiCoO_2$ [1,12,13]. However, $LiNiO_2$ suffers from an intrinsic poor thermal stability at a fully charged state with a poor cycle life, and these characteristics are related to the chemical and structural instability of tetravalent nickel [14,15]. Comparatively, nickel-rich layered $Li(Ni_{1-x-y}Mn_xCo_y)O_2$, which has a partial substitution of Co and Mn for Ni, is a promising material because of its lower cost, reduced toxicity, improved thermal stability, and good cycling stability and safety. A series of these materials shows that Ni can achieve a high capacity while Co provides a higher electrical conductivity and rate performance. Mn is associated with the cycling performance because a part of Mn does not change its valence state during charge and discharge cycles [14,16,17]. Various methods have been applied in the synthesis of Ni-rich layered cathode materials, including solid state [18], sol-gel [19-22], chloride co-precipitation [23], carbonate co-precipitation [19,24] and hydroxide co-precipitation [15,25-30] methods. A comparison of these synthesis methods shows that the co-precipitation method has many advantages in that it provides a homogeneous precursor with high tap-density, a uniform distribution for the Ni, Co, and Mn atoms, a controllable morphology, improved electrochemical properties and favorable process conditions for mass production. Ying et al. [31] prepared $LiNi_{0.8}Co_{0.2}O_2$ via co-precipitation and obtained a charge capacity of 217 mAh g^{-1} followed by a discharge capacity of 172 mAh g^{-1} and a 79.3% Coulombic efficiency during the initial cycle. Cheralathan et al. [32] also investigated the effect of the preparation conditions, such as the pH, NH_4OH concentration and co-precipitation time, to synthesize micro-spherical $LiNi_{0.8}Co_{0.15}Mn_{0.05}O_2$ materials. Spherical $LiNi_{0.8}Co_{0.15}Mn_{0.05}O_2$ prepared under optimum conditions exhibited a hexagonally-ordered, layered structure and an initial charging capacity of 176 $mAhg^{-1}$ without cation mixing. More than 91% of the initial capacity was retained after 40 cycles at a 1 C-rate in a voltage range from 3.0 to 4.3 V.

In this work, we have successfully synthesized layered Ni-rich $LiNi_{0.8}Co_{0.1}Mn_{0.1}O_2$ material. The synthesis conditions for spherical $Ni_{0.8}Co_{0.1}Mn_{0.1}(OH)_2$ precursors, such as the pH, the ratio of the chelating agent (NH_4OH) to metal solution, the stirring speed, temperature and residence time have been studied in detail. These materials were synthesized through continuous co-precipitation by using a continuously stirred tank reactor (CSTR). The properties of the $Ni_{0.8}Co_{0.1}Mn_{0.1}(OH)_2$ precursor and the electrochemical prop-

†To whom correspondence should be addressed.
E-mail: jwlee7@dankook.ac.kr
‡This paper is submitted as a contribution to celebrating the honorable retirement of Prof. Hwayong Kim of Seoul National University.

Table 1. Synthetic conditions of the precursors

Sample	pH	NH_4OH : metal	Rotation speed/ rpm	Temperature/ °C	Residence time/h
P_1	11.2	1 : 1	600	50	10
P_2	11.5	1 : 1	600	50	10
P_3	11.8	1 : 1	600	50	10
P_4	11.5	0.8 : 1	600	50	10
P_5	11.5	1.2 : 1	600	50	10
P_6	11.5	1 : 1	500	50	10
P_7	11.5	1 : 1	800	50	10
P_8	11.5	1 : 1	600	45	10
P_9	11.5	1 : 1	600	55	10
P_{10}	11.5	1 : 1	600	50	8
P_{11}	11.5	1 : 1	600	50	12

erties of the $LiNi_{0.8}Co_{0.1}Mn_{0.1}O_2$ materials were also investigated.

EXPERIMENTAL

1. Materials Synthesis

The layered oxide $LiNi_{0.8}Co_{0.1}Mn_{0.1}O_2$ powders were prepared via co-precipitation [32]. At first, a stoichiometric amount of $NiSO_4 \cdot 6H_2O$, $CoSO_4 \cdot 7H_2O$, and $MnSO_4 \cdot 6H_2O$ with the corresponding molar composition of 0.8 : 0.1 : 0.1 were dissolved together in de-ionized water to obtain a transparent solution. The solution was then pumped into a continuously stirred tank reactor (CSTR, capacity 1.5 L) under an N_2 atmosphere. At the same time, the NaOH and NH_4OH solutions were separately pumped into the reactor. The optimum synthetic (co-precipitation) conditions were investigated in detail, and these conditions are summarized in Table 1. In general, the particle size and the morphology are the most important factors that determine the performance of the cathode material. We adjusted the corresponding parameters, including the pH, molar ratio of NH_4OH to the metal solution, reaction temperature, stirring speed, and residence time, because these have a great effect on the particle size and on the morphology of the materials. The co-precipitated spherical $Ni_{0.8}Co_{0.1}Mn_{0.1}(OH)_2$ powder was filtered, washed with de-ionized water and vacuum-dried at 110 °C for 24 h. Finally, the $Ni_{0.8}Co_{0.1}Mn_{0.1}(OH)_2$ precursors were mixed with $LiOH \cdot H_2O$ (with a molar ratio of Li/M=1.05), preheated to 480 °C for 5 h and then heated at 780, 800, and 820 °C for 16 h in air to obtain the $LiNi_{0.8}Co_{0.1}Mn_{0.1}O_2$ powder.

2. Material Characterization

The crystalline structure of the samples was characterized via X-ray diffraction (XRD) measurements using a Rigaku D Max/ 2000 PC with Cu Kα radiation in the 2θ angular range of 10 to 80° at a scanning rate of 4° min^{-1}. The particle morphology and the elemental composition of the powder were assessed using a scanning electron microscope (SEM, Hitachi S-4800) equipped with an energy dispersive spectroscope (EDS).

3. Electrochemical Characterization

2016 coin-type cells were used to measure the electrochemical properties of the samples. The cells were cycled galvanostatically between 3.0 V and 4.3, 4.5 and 4.7 V. The cathodes that were used during the cell test were fabricated with a mixture of the active material (80 wt%), conductive agent (Super P, Timcal) (10 wt%), and polyvinylidene fluoride (PVDF, KF 1300, KUREHA) binder (10 wt%) by dispersion/dissolution in N-methyl-2-pyrrolidene (NMP). We prepared the cathode slurry by mixing the NMP solution with the polyvinylidene fluoride, the carbon black, and the powdery cathode-active material. To prepare the electrodes, the cathode slurry was coated on an Al foil, left to dry at 110 °C for 8 h in a vacuum oven, and then roll-pressed prior to use. All electrodes were cut into disks with diameters of 1.4 cm. The electrochemical measurements were carried out with coin-type cells (CR-2016 size) containing the cathode, a Li-metal anode (as a counter electrode), a micro-porous polyethylene separator (E16MMS, Tonen), and 1 : 2 volume ratio mixture of ethylene carbonate (EC) and ethylene methyl-carbonate (EMC) containing 1 M $LiPF_6$ as electrolyte (PANAX, ETEC Co., Ltd., Korea). The cells were prepared in an Ar-filled glove box in which oxygen and H_2O content remained below 1.0 ppm.

The cells were tested using a cycler (PNE solution, KOREA) in the potential range from 3.0 to 4.3 V at different current densities ranging from 18.5 mA g^{-1} (0.1C) to 1,295 mA g^{-1} (7C) at room temperature (25 °C) and at 60 °C. Cyclic voltammetry (CV) measurements were then conducted in a voltage range from 3.0 to 4.3 V at a scanning rate of 0.1 mV s^{-1} by using an electrochemical analyzer (Bio-logic, VSP, France).

RESULTS AND DISCUSSION

1. Characteristics of the $Ni_{0.8}Co_{0.1}Mn_{0.1}(OH)_2$ Precursors

The synthesis conditions for the precursors are highly important because they affect the morphology, phase structure and electrochemical properties of the materials. Fig. 1 shows the SEM images of the $Ni_{0.8}Co_{0.1}Mn_{0.1}(OH)_2$ powders (P_1, P_2 and P_3) that were prepared at different pH values. The pH value also plays an important role in determining the purity of the manganese hydroxide precipitation because the formation of manganese oxides may be promoted by increasing the pH [33]. When the pH is 11.5, the particles are nearly uniform in shape [Fig. 1(b)] and the tap-density of the precursor is 1.91 g cm^{-3}. The particle shape of the precursor is spherical, and the average secondary particle diameter (D_{50}) is 16 μm with a primary particle that is smaller than 500 nm. When the pH increases, the particles become smaller and non-uniform, and a lot of fine particles can be observed [Fig. 1(c)]. The tap-density thus gradually decreases as the pH increases (1.26 g cm^{-3} at pH=11.8). Therefore, the pH was fixed at 11.5 for the following experiments.

NH_4OH is a well-known chelating agent used in the co-precipitation method, and this material prevents phase separation and promotes the formation of homogeneous transition metal hydroxide [24,34]. The molar ratio of the transition metal to NH_4OH also influences the morphology and the microstructure, as can be clearly observed in Fig. 2. The primary crystalline grains become smaller when the molar ratio of NH_4OH to metal increases, and at a molar ratio of 1.0, the surface morphology of particles becomes sheet-like and the secondary particles are observed to be more uniform than the others. In addition, when the molar ratio of NH_4OH to transition metal increases, the concentration of the complex $[Ni(NH_3)_n]^{2+}$ in-

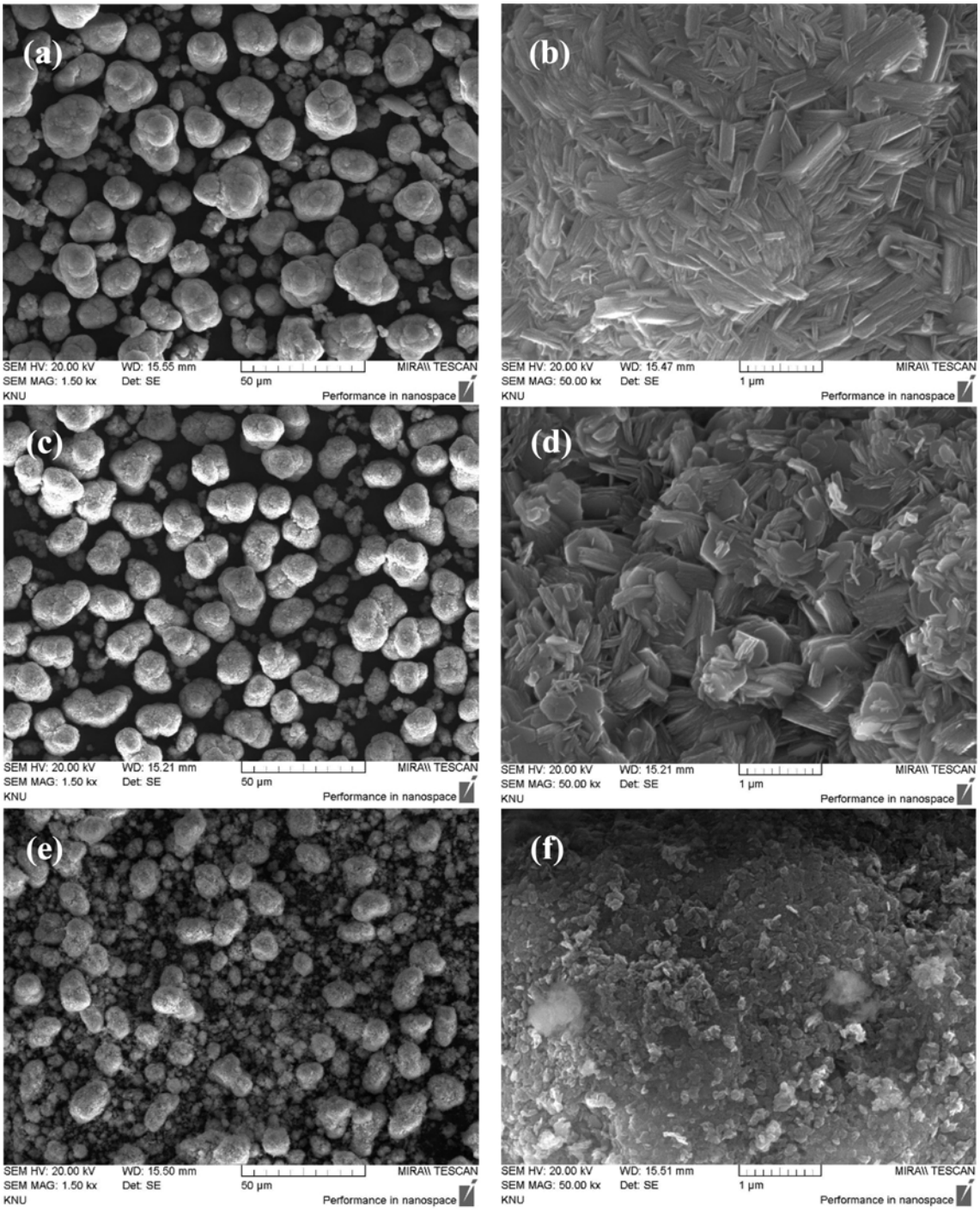

Fig. 1. SEM images of $Ni_{0.8}Co_{0.1}Mn_{0.1}(OH)_2$ powders prepared at various pH. (a), (b) P_1 11.2; (c), (d) P_2 11.5; and (e), (f) P_3 11.8 (magnification: I=1,500× and II=50,000×).

creases, which leads to an incomplete precipitation of Ni^{2+} [33].

The stirring speed was adjusted to examine the effect of the stirring speed on the particle morphology. Highly agglomerated particles can be observed at a relatively low stirring speed (Fig. 3(a)). At a low stirring speed (500 rpm), the particles become larger than those that were obtained at a high stirring speed. The spherical particles of the 3 precursors that were obtained at stirring speeds of 500, 600 and 800 rpm have an average size of approximately 20, 16 and 13 µm, respectively. It is thus clear that the stirring speed greatly affects size of the particles of the precursor.

The effect of the reaction temperature is investigated by fixing the pH, the molar ratio of NH_4OH to metal and the stirring speed to the optimum values that have been previously determined. The morphology of the precursor particles is shown in Fig. 4. The highest purity and uniformity of the particle size and morphology were achieved at a 50 °C co-precipitation temperature. The tap-density

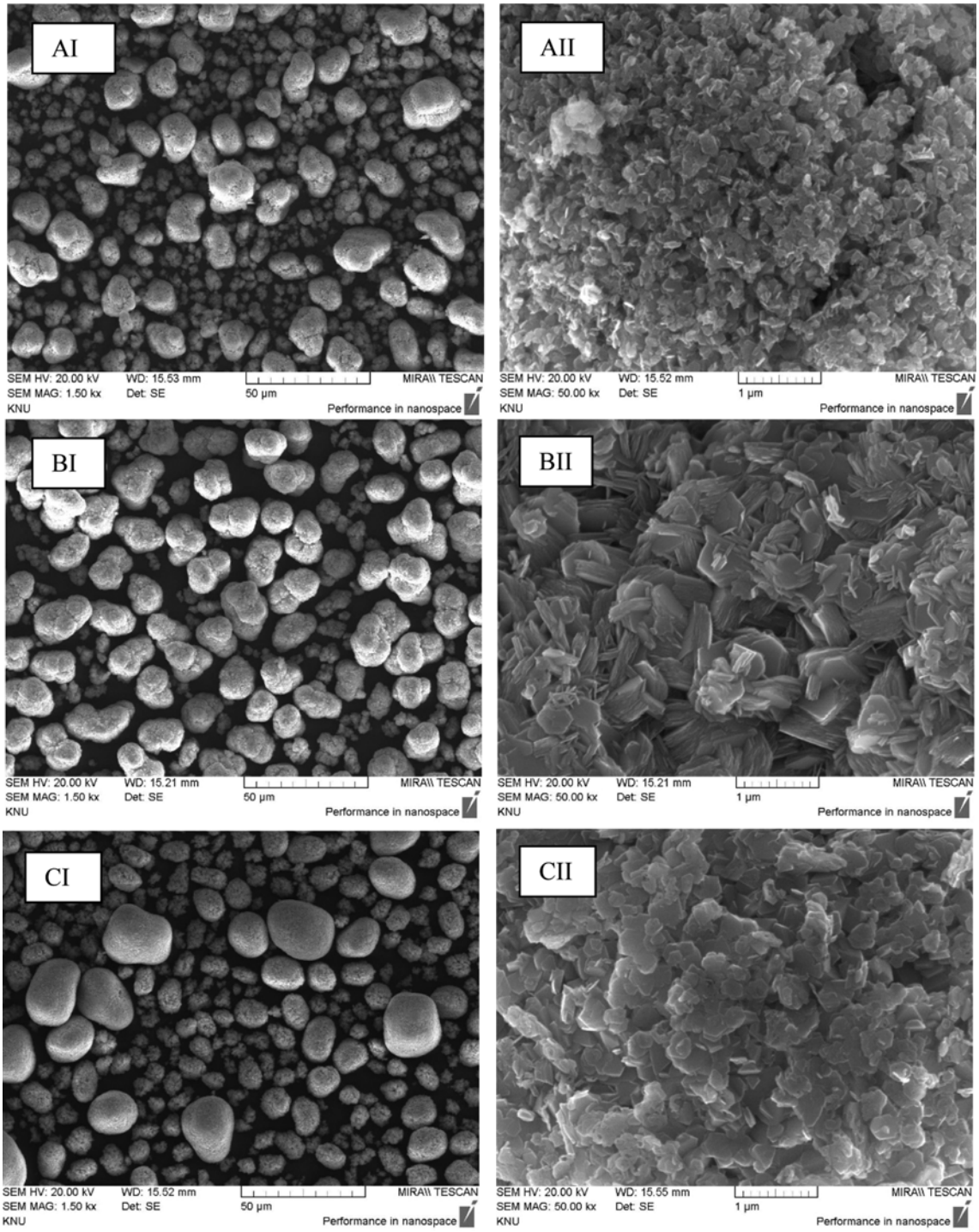

Fig. 2. SEM images of $Ni_{0.8}Co_{0.1}Mn_{0.1}(OH)_2$ powders prepared at various molar ratios of NH_4OH/metal: (a) P_4 0.8, (b) P_2 1.0, and (c) P_5 1.2 (magnification: I=1,500× and II=50,000×).

of the samples does not change significantly with variations in the reaction temperature. At 45 °C, the precursor has a smaller primary particle size and a lower tap-density than those obtained at 50 and 55 °C. Liang et al. reported that the purity of the particles becomes lower at higher temperatures than 50 °C which may be a result of the presence of MnOOH or Mn_3O_4 impurities [28]. The stability of transition metal ions that are chelated by ammonium ions may also decrease as the co-precipitation temperature increases.

Finally, the effect of the residence time was investigated. The definition of the residence time is described in Eq. (1):

$$\tau = \frac{V}{q} \tag{1}$$

where τ is the residence time, V is the volume of the reactor, and q

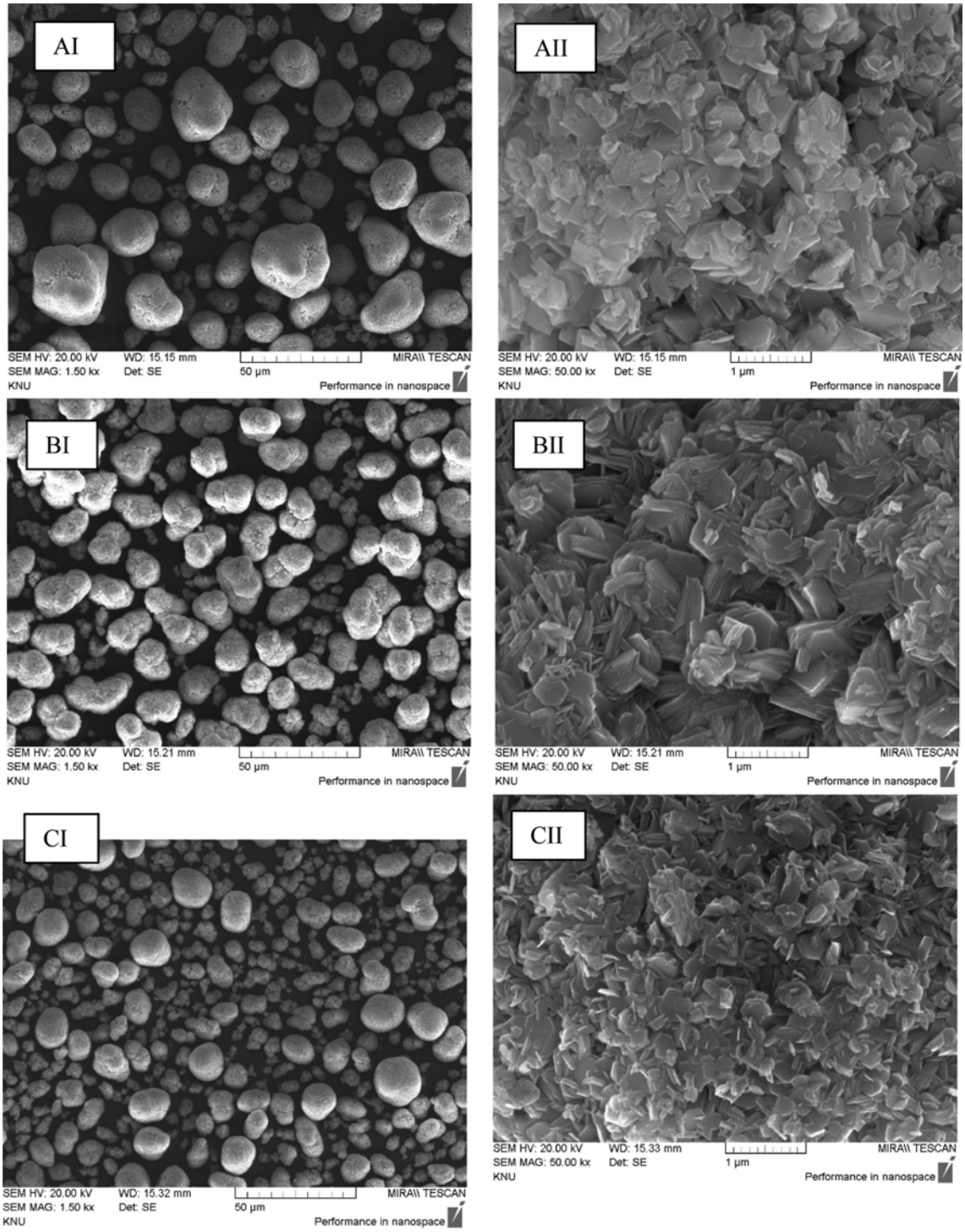

Fig. 3. SEM images of $Ni_{0.8}Co_{0.1}Mn_{0.1}(OH)_2$ powders prepared at various stirring speed. (a) P_6 500 rpm; (b) P_2 600 rpm; and (c) P_7 800 rpm (magnification: I=1,500× and II=50,000×).

is the flow rate of the reactants. In this study, the residence times were adjusted to 8 h, 10 h, and 12 h, and the SEM images of the particles that were obtained for each residence time are shown in Fig. 5. For a residence time of 8 h and 10 h, the particle size and the morphology are similar. However, as the residence time is further elongated (12 h), the particle size becomes smaller (9.18 μm) and non-uniform. The primary particles are also smaller and exhibit sheet-like nano-plates on the surface. Secondary particles are composed of aggregated primary particles, and the long residence time (low flow rate of the reactants) decreases the degree of supersaturation and hinders the aggregation process, which may be the reason for which smaller secondary particles are obtained at a long residence time.

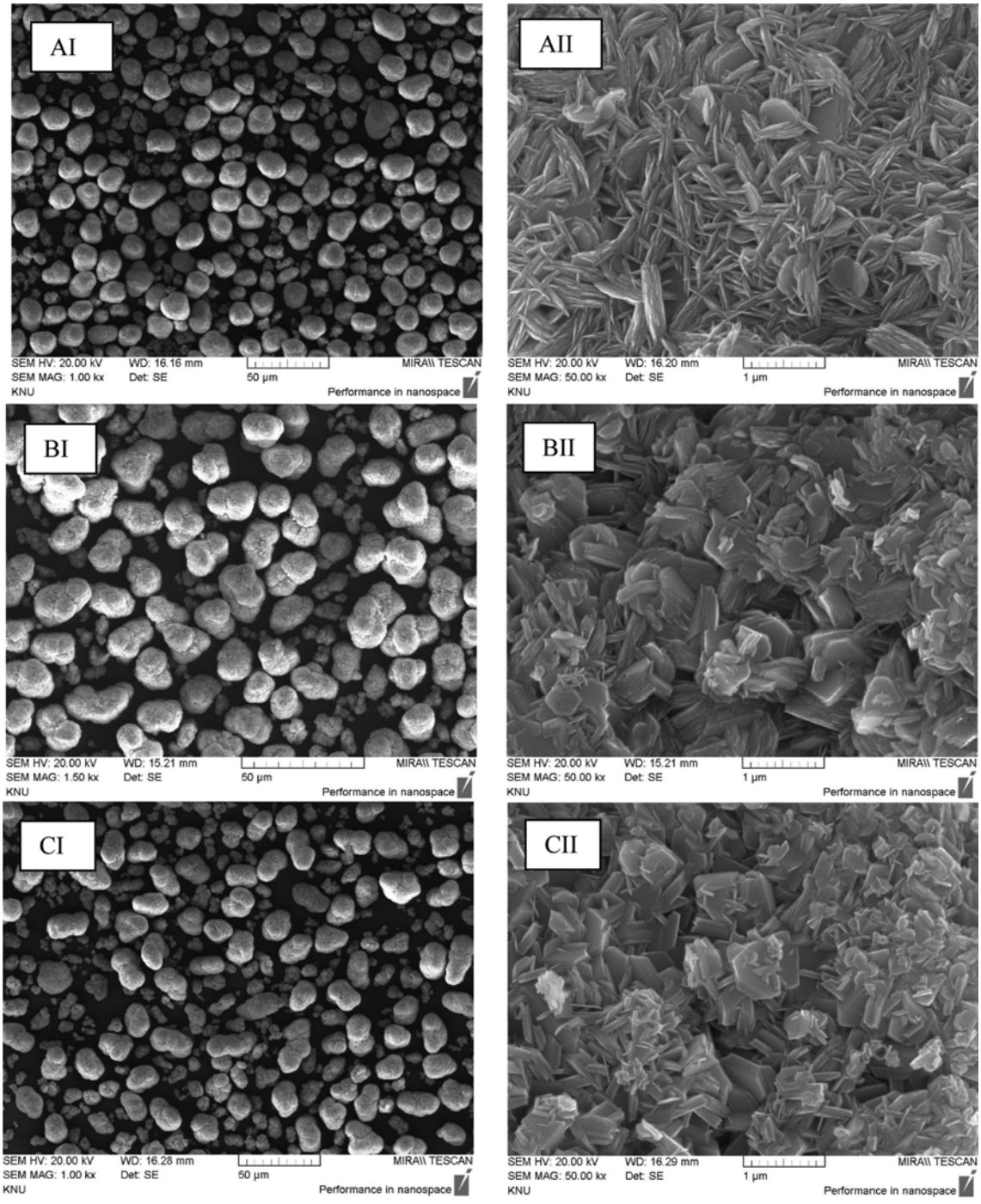

Fig. 4. SEM images of $Ni_{0.8}Co_{0.1}Mn_{0.1}(OH)_2$ powders prepared at various reaction temperature. (a) P_8 45 °C; (b) P_2 50 °C; and (c) P_9 55 °C (magnification: I=1,000× and II=50,000×).

2. Characteristics of the $LiNi_{0.8}Co_{0.1}Mn_{0.1}O_2$ Powder

The spherical $Ni_{0.8}Co_{0.1}Mn_{0.1}(OH)_2$ precursor (P_2 sample) is then used to investigate the relationship between the synthesis temperature and the physical/electrochemical properties of the $LiNi_{0.8}Co_{0.1}Mn_{0.1}O_2$ cathode materials that were lithiated via calcination at various temperatures from 780 to 820 °C.

Fig. 6(a) shows the X-ray diffraction pattern of the $Ni_{0.8}Mn_{0.1}Co_{0.1}(OH)_2$ precursor (P_2 sample), which is similar to that of $Ni(OH)_2$ [31]. All of the diffraction lines are indexed to a hexagonal structure with a space group of $P\bar{3}m1$. The crystal lattice parameters of the layered $Ni_{0.8}Mn_{0.1}Co_{0.1}(OH)_2$ precursor are a=3.114 Å and c=4.617 Å. Fig. 6(b) displays the XRD patterns of the $LiNi_{0.8}Co_{0.1}Mn_{0.1}O_2$ samples that were prepared by calcining the precursor and $LiOH{\cdot}H_2O$ mixture at 780, 800, and 820 °C for 16 h. The XRD patterns exhibit clear peak splits of 006/102 and 108/110 doublets, which indicate that the materials have a well-ordered crystalline struc-

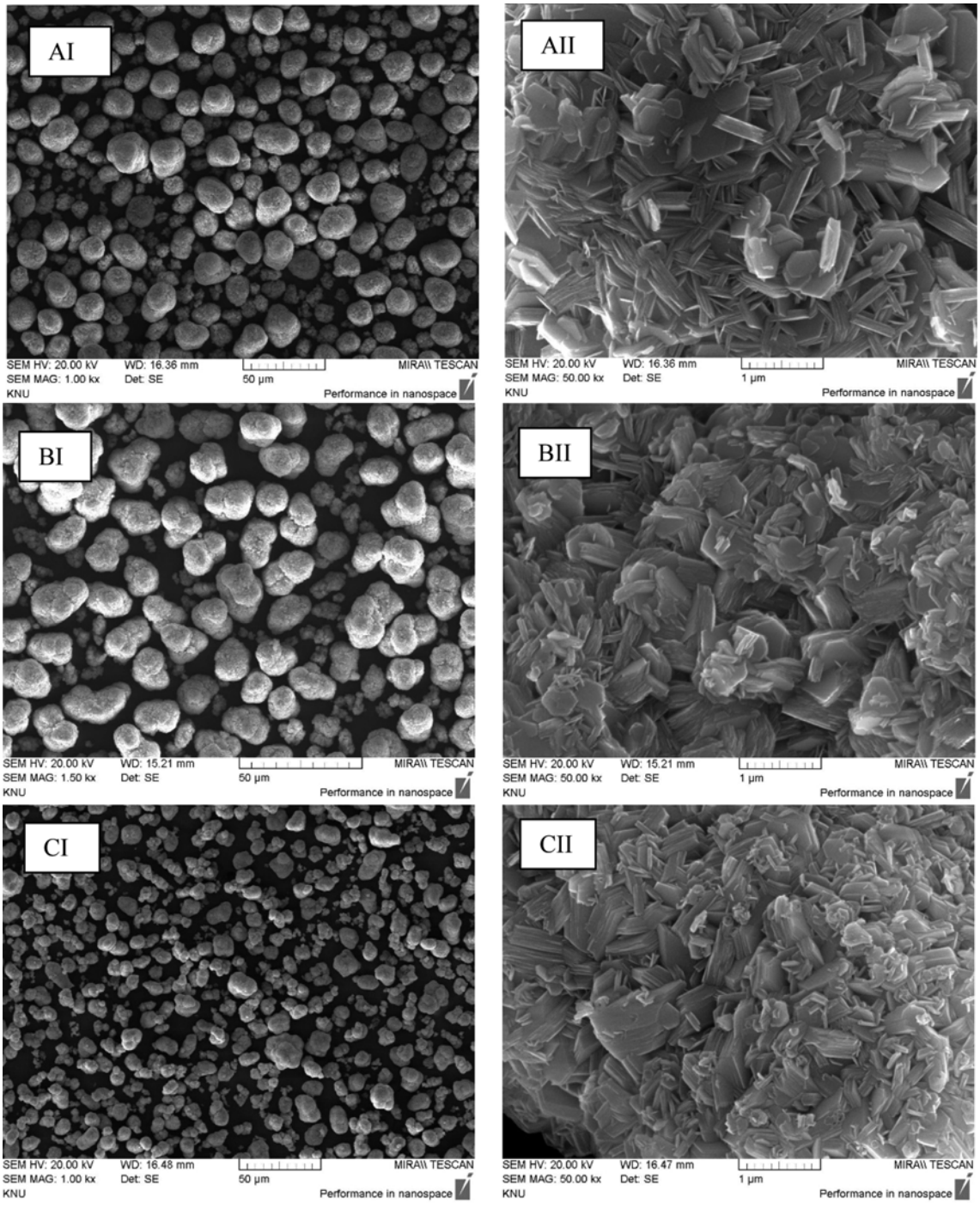

Fig. 5. SEM images of $Ni_{0.8}Co_{0.1}Mn_{0.1}(OH)_2$ powders prepared at various residence time. (a) P_{10} 8 h; (b) P_2 10 h; and (c) P_{11} 12 h (magnification: I=1,000× and II=50,000×).

ture. All of the diffraction peaks are indexed to an α-$NaFeO_2$ structure ($R\bar{3}m$), and no impurity peaks appear. The unit cell parameters are calculated and summarized in Table 2. The 'a' cell parameter is the measure of the intralayer metal-metal distance and the 'c' parameter is the sum of the MO_6 (M=transition metal) octahedra layer (slab) thickness (slab thickness S) and LiO_6 octahedra layer thickness (interslab thickness I) in the lamellar structure of $LiMO_2$ [35]. Therefore, the increase in the parameter reflects an increase in the effective ionic radius. From Table 2, the lattice parameters a and c increase from 2.8733 Å and 14.2123 Å to 2.8751 and 14.2217 Å, respectively, as the calcination temperature increases. The values of c/a for all samples are relatively high, which indicates the formation of a well-ordered layered structure [35,36]. In the material with a layer-structure, cation mixing is known to negatively impact the electrochemical performance. The intensity ratio of I_{003}/I_{104} is an indicative parameter to determine the cation mixing in the lat-

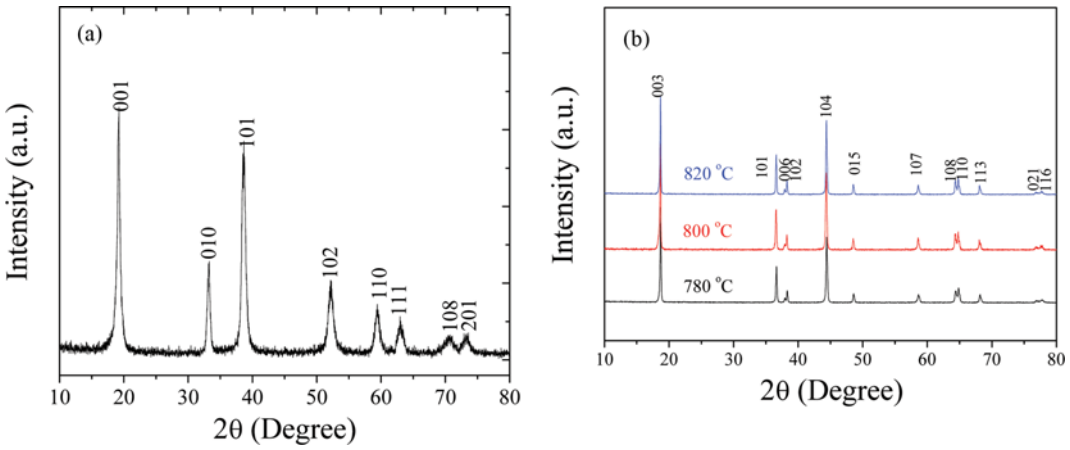

Fig. 6. XRD pattern for (a) $Ni_{0.8}Mn_{0.1}Co_{0.1}(OH)_2$ (P_2 sample) powders and (b) $LiNi_{0.8}Co_{0.1}Mn_{0.1}O_2$ samples prepared at various calcination temperatures: 780, 800 and 820 °C.

Table 2. Comparison of the lattice parameters of $LiNi_{0.8}Co_{0.1}Mn_{0.1}O_2$ samples at various calcination temperatures

	a (Å)	c (Å)	c/a	R_w	R_f
$LiNi_{0.8}Co_{0.1}Mn_{0.1}O_2$ - 780 °C	2.8733	14.2123	4.9463	1.4438	0.5068
$LiNi_{0.8}Co_{0.1}Mn_{0.1}O_2$ - 800 °C	2.8753	14.2192	4.9419	1.3831	0.5068
$LiNi_{0.8}Co_{0.1}Mn_{0.1}O_2$ - 820 °C	2.8751	14.2217	4.9464	1.3327	0.5366

tice of the layered oxides [37,38], and a value lower than 1.2 indicates a higher degree of cation mixing [39]. Table 2 shows that the I_{003}/I_{104} ratios of all samples are greater than 1.2, which indicates that all samples have a well-ordered layered α-$NaFeO_2$ structure. The I_{003}/I_{104} ratio is 1.4438, 1.3831 and 1.3327 at 780, 800 and 820 °C, respectively. The results also indicate that the $LiNi_{0.8}Co_{0.1}Mn_{0.1}O_2$ samples synthesized at 780 and 800 °C have better-ordered layered structures, with lower Ni^{2+} and Li^+ anti-site disordering than the other sample [39].

The morphology of the $LiNi_{0.8}Co_{0.1}Mn_{0.1}O_2$ samples obtained at various calcination temperatures are shown in Fig. 7. The spherical particle shape and the average particle diameter are almost same as those of the precursors after calcination. However, the sheet-like primary particles of the precursor can be seen to have completely changed into rectangular primary particles with sizes of 0.5 to 1 μm (Fig. 7). This indicates that the size and the shape of the secondary particles do not change significantly during calcination while only the primary particles exhibit a change in morphology, resulting in an improvement of the tap-density (2.35 g cm^{-3}). At 800 °C, the primary particles are the smallest relative to other samples, which would then result in a large specific area of the sample and an improvement in the rate capability.

Fig. 8 shows the corresponding elemental mapping images of the cathode materials that were acquired with energy dispersive X-ray spectroscopy (EDX). Ni, Co, and Mn elements are seen to have a uniform distribution over the particles. The atomic ratio of Ni : Co : Mn in the sample is measured to be 0.812 : 0.105 : 0.0826 (Table 3), which is close enough to our target composition of 8 : 1 : 1, considering that the EDX can give only an approximate composition.

3. Electrochemical Properties

The initial charge-discharge curves of the $LiNi_{0.8}Co_{0.1}Mn_{0.1}O_2$ samples that were calcined at various temperatures are shown in Fig. 9(a). The $LiNi_{0.8}Co_{0.1}Mn_{0.1}O_2$ electrodes were discharged at a 0.1 C-rate in the voltage range from 3.0 to 4.3 V at 25 °C and 60 °C. The discharge capacities increase as the calcination temperature increases from 780 to 800 °C. The initial discharge capacity for the samples calcined at 780, and 800 °C are 185.6 and 193.9 mAh g^{-1}, respectively. However, the discharge capacity decreases to 186.2 mAh g^{-1} when the calcination temperature increases to 820 °C. Although calcination at a higher temperature can increase the crystallinity, excessive lithium evaporation is unavoidable during heat treatment [40]. For the cell test at an elevated temperature (60 °C), the $LiNi_{0.8}Co_{0.1}Mn_{0.1}O_2$ calcined at 800 °C exhibits an initial discharge capacity of 211.1 mAh g^{-1}. The cycling performance of the $LiNi_{0.8}Co_{0.1}Mn_{0.1}O_2$ calcined between 780 and 820 °C at a constant current density of 185 mA g^{-1} (approximately 1 C) was also investigated, and the results are shown in Fig. 9(b). The cell delivers a capacity of 170.4 mAh g^{-1} at the 1st cycle and 153.7 mAh g^{-1} at the 100th cycle with a capacity retention of 90.41% while the samples calcined at 780 and 820 °C exhibited a capacity retention of 84.5 and 80.9%, respectively. In the high-temperature cycling test (60 °C), the cell delivers a capacity of 196.6 mAh g^{-1} at the 1st cycle and 156.4 mAh g^{-1} at the 100th cycle, with a capacity retention rate of 79.6%. The poor capacity retention for $LiNi_{0.8}Co_{0.1}Mn_{0.1}O_2$ is characteristic of Ni-rich cathode materials due to the structural transformation near the surface region. The spontaneous reduction of Ni^{3+} to stable Ni^{2+} and the evolution of oxygen species from the surface also contributes to the formation of LiOH and Li_2CO_3 on the surface [18,41].

The cycling stability at a higher voltage was observed by increasing the upper cut-off voltage to 4.5 and 4.7 V vs. Li^+/Li for the $LiNi_{0.8}Co_{0.1}Mn_{0.1}O_2$ calcined at 800 °C. Fig. 10(a) shows that the initial discharge capacities gradually increase when the upper cut-off volt-

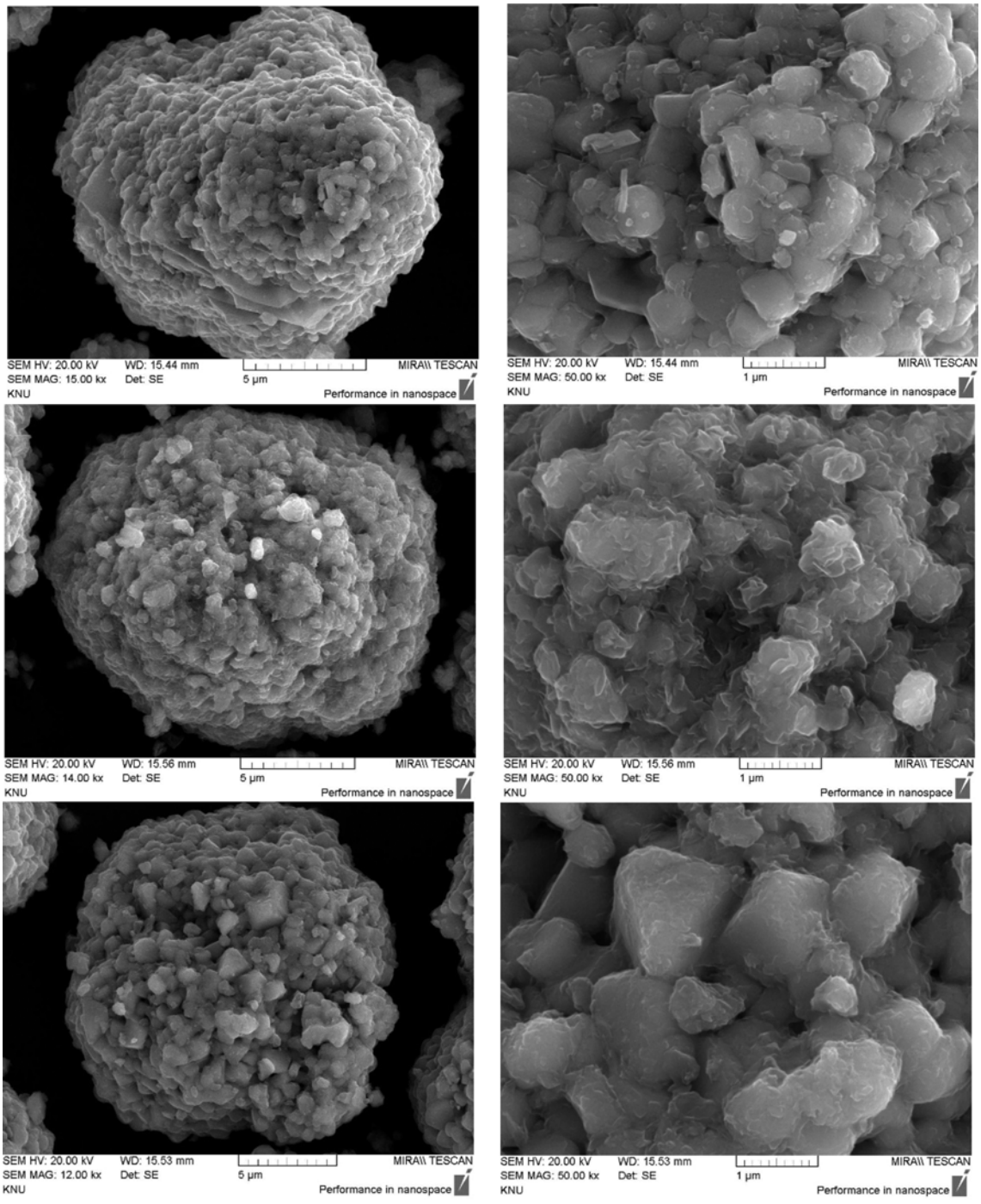

Fig. 7. SEM images of $LiNi_{0.8}Co_{0.1}Mn_{0.1}O_2$ sample prepared at various calcination temperatures (a) 780, (b) 800 and (c) 820 °C.

age is raised. In the voltage range from 3.0 to 4.3, 4.5 and 4.7 V, the initial discharge capacities of the $LiNi_{0.8}Co_{0.1}Mn_{0.1}O_2$ samples are 193.9, 210.4 and 217.7 mAh g^{-1}, respectively. The cycling stability of the $LiNi_{0.8}Co_{0.1}Mn_{0.1}O_2$ electrode is shown in Fig. 10(b). The discharge capacity gradually decreases from 170.4 mAh g^{-1} at the 1st cycle (1 C-rate) to 153.7 mAh g^{-1} at the 100th cycle with a capacity retention of 90.4% over 3.0 to 4.3 V. For cycling with 4.5 and 4.7 V of the upper cut-off voltage, only 43.8 and 47.8% of the initial capacity was retained at the 100th cycle. This severe capacity fading at a high cut-off voltage may be a result of the interfacial reaction between the electrolyte and the cathode material and a dissolution of the cobalt at a high operating potential (>4.3 V), which can lead to a significant degradation in the capacity retention [42,43].

The rate capability is well-known to be strongly affected by the surface area and the primary particle size of the cathode material. Fig. 11 shows the rate performance of the $LiNi_{0.8}Co_{0.1}Mn_{0.1}O_2$ calcined at 800 °C, as measured at various current densities in the voltage range from 3.0 to 4.3 V. The cells were cycled at 0.1 C (18.5 mA

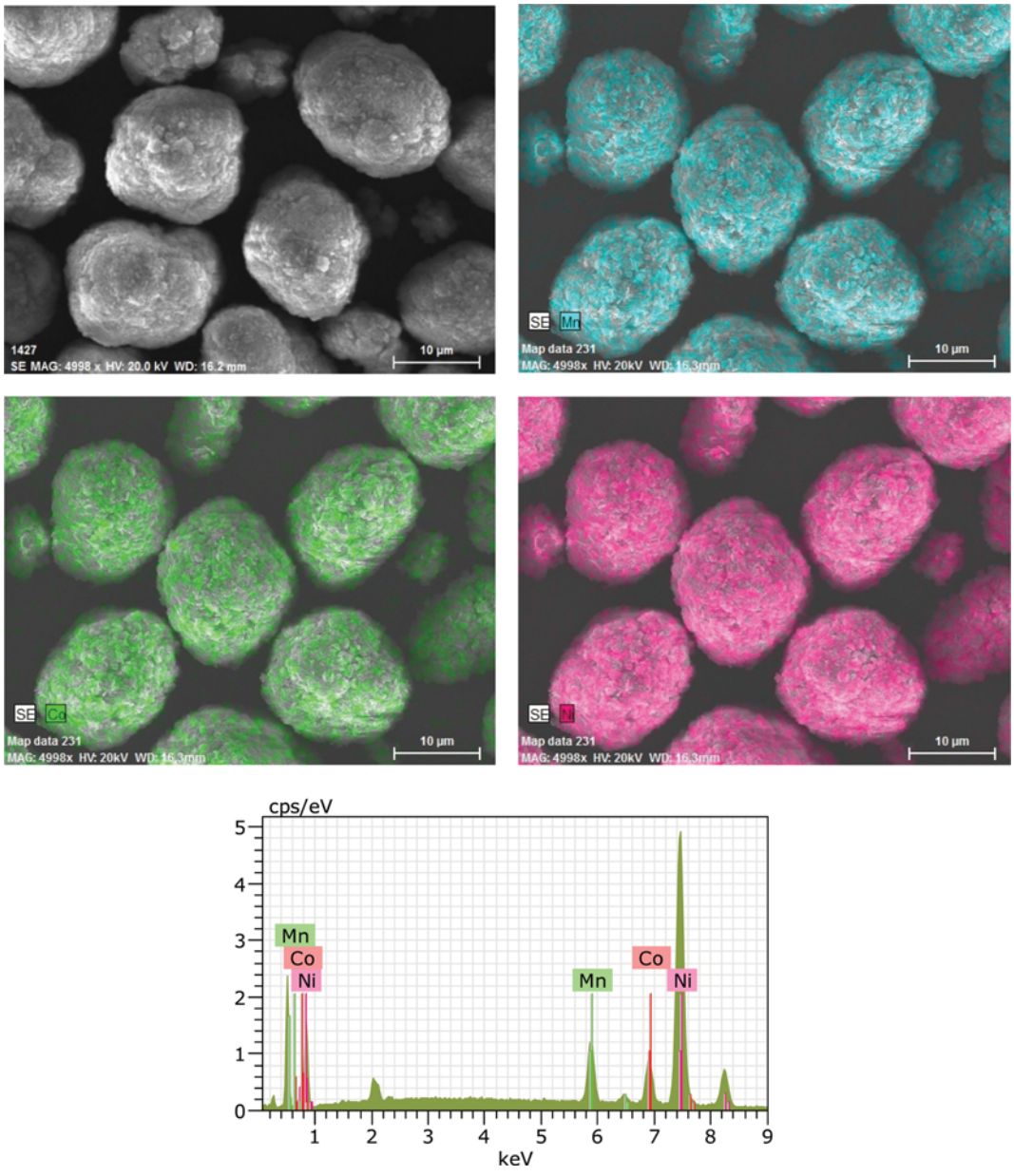

Fig. 8. Elemental mapping images and EDX analysis of $LiNi_{0.8}Co_{0.1}Mn_{0.1}O_2$ prepared at 800 °C.

Table 3. EDX analysis of $LiNi_{0.8}Co_{0.1}Mn_{0.1}O_2$ prepared at 800 °C

Element	Norm. C [wt%]	Atom. C [at%]
Nickel	81.64	81.24
Cobalt	10.59	10.5
Manganese	7.77	8.26

g^{-1}) for 5 cycles, then at 0.2 C (37 mA g^{-1}), 0.5 C (92.5 mA g^{-1}), 1 C (185 mA g^{-1}), 3 C (555 mA g^{-1}), 5 C (925 mA g^{-1}), 7 C (1,285 mA g^{-1}) and finally returning to 0.1 C (18.5 mA g^{-1}) each for 5 cycles. The $LiNi_{0.8}Co_{0.1}Mn_{0.1}O_2$ represents a good rate capability, as shown in the figure. Even at the 7 C-rate, the sample showed a capacity as high as 130.7 mAh g^{-1} (68.8% of the capacity retention vs. 0.1 C), indicating that the $LiNi_{0.8}Co_{0.1}Mn_{0.1}O_2$ synthesized in optimum conditions has a superior rate capability that has not been attained in prior studies [19,25,26]. The above results indicate that the $LiNi_{0.8}Co_{0.1}Mn_{0.1}O_2$ synthesized via co-precipitation with optimum conditions (pH=11.5, 600 rpm, 50 °C and 1.0 molar ratio of NH_4OH/metal solution) exhibit the highest initial capacity and a good rate capability. However, the cycling performance still needs to improve.

Cyclic voltammetry (CV) was carried out for the initial three cycles between 3.0 and 4.3 V at a scan rate of 0.1 mV·s^{-1} in order to investigate the structural stability of the $LiNi_{0.8}Co_{0.1}Mn_{0.1}O_2$ materials against the electrochemical reaction, and the results are shown in Fig. 12. The CV profile of the first cycle can be seen to differ from those of the following cycles. The anodic peaks were observed at 3.94 and 4.24 V during the first delithiation; at 3.83, 4.02 and

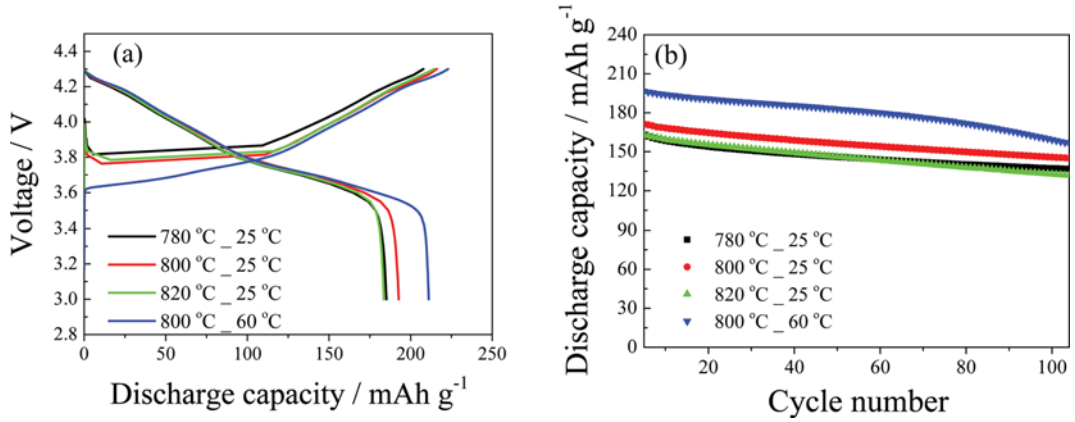

Fig. 9. Electrochemical performance of the $LiNi_{0.8}Co_{0.1}Mn_{0.1}O_2$ prepared at 800 °C in a voltage range of 3.0-4.3 V at 25 and 60 °C. (a) First charge–discharge curves at a rate of 0.1 C and (b) discharge capacity vs. cycle number at 1 C.

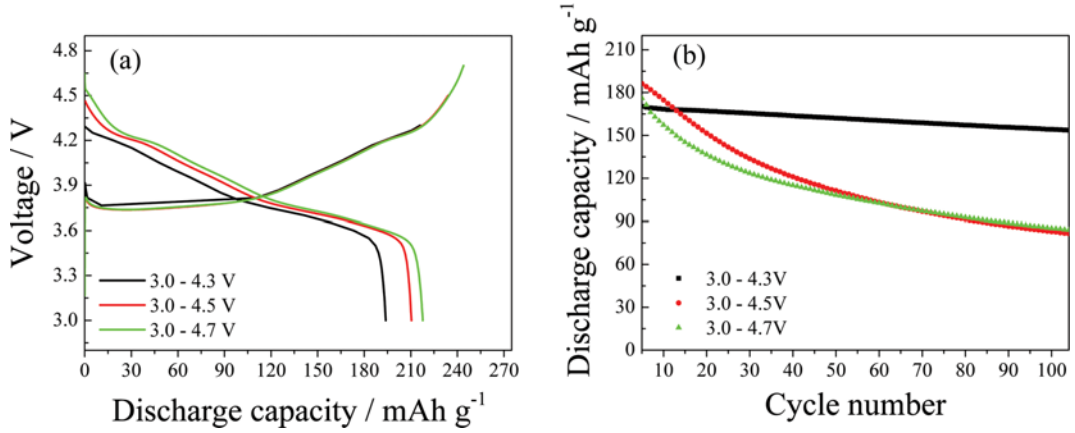

Fig. 10. Electrochemical performance of the $LiNi_{0.8}Co_{0.1}Mn_{0.1}O_2$ prepared at 800 °C with an upper cut-off voltage of 4.3, 4.5, and 4.7 V at 25 °C. (a) First charge–discharge curves at a rate of 0.1 C and (b) discharge capacity vs cycle number at 1 C, at 4.3, 4.5 and 4.7 V, respectively.

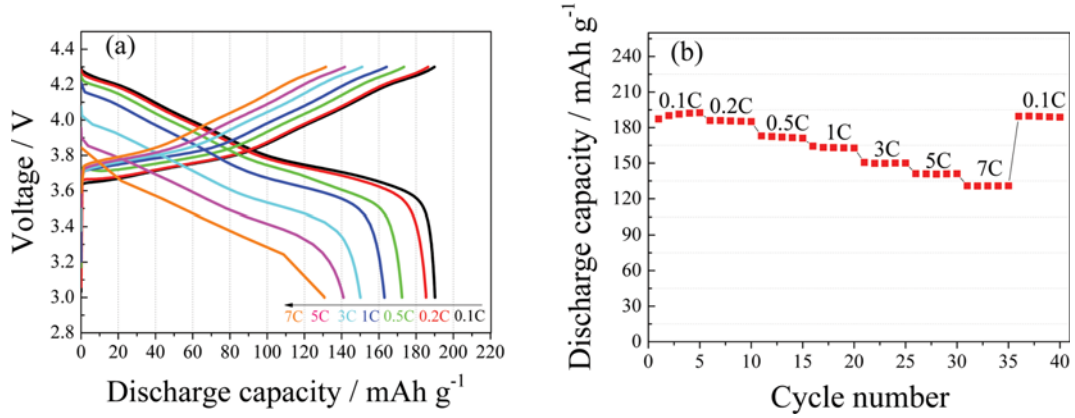

Fig. 11. Electrochemical performance of the $LiNi_{0.8}Co_{0.1}Mn_{0.1}O_2$ prepared at 800 °C in a voltage range of 3.0-4.3 V at 25 °C. (a) Initial charge–discharge curves and (b) rate capability measured at 0.1 to 7 C of discharge current density. The electrodes were charged at 0.1 C and discharged at the corresponding rates.

4.25 V during the second delithiation; at 3.83, 4.02 and 4.25 V during the third delithiation; and at 3.82, 4.02 and 4.25 V during the fourth delithiation. In the first anodic scan, there is a prominent anodic reaction at 3.94 V, but it is no longer observed during the subsequent cycles. This may be attributed to the activation of the electrode after which the potential of the delithiation reaction de-

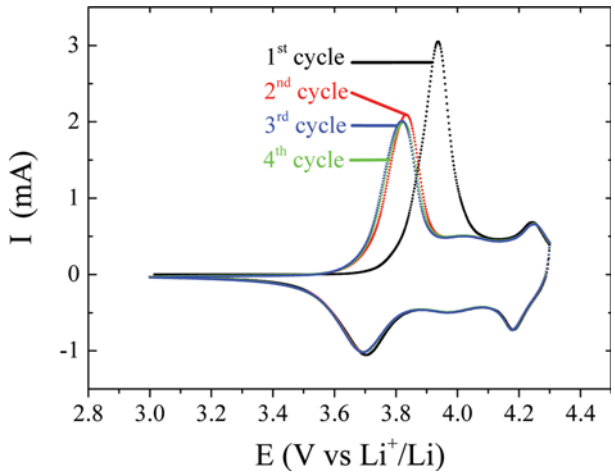

Fig. 12. Cyclic voltammetry (0.1 mV s^{-1}, 3.0-4.3 V) of $LiNi_{0.8}Co_{0.1}Mn_{0.1}O_2$ prepared at 800 °C.

creases [44]. Lu et al. [19] reported that the first oxidation peak corresponds to the transformation of the material from a pristine hexagonal phase (H_1) to a new monoclinic phase (M), the second corresponds to the transformation between the monoclinic phase and the second hexagonal phase (H_2), and the last corresponds to an H_2 transformation to a third hexagonal phase (H_3). Due to the complicated phase transformations during charge and discharge cycles, the material often shows an unstable cycle life performance. Furthermore, the high concentration of unstable Ni^{4+} in the delithiated state (H_3 phase) can be easily reduced to a divalent and insulating NiO phase at the surface [39,45], which would also result in capacity fading during cycling, which helps to understand why the material often faces a rapid loss in capacity during cycling. There is no obvious difference in the redox peak (3.82 V of cathodic peak potential and 3.69 V of anodic peak potential), which indicates that the Li-ions are reversibly intercalated and de-intercalated in the $LiNi_{0.8}Co_{0.1}Mn_{0.1}O_2$ electrode with good stability.

CONCLUSIONS

1) Homogeneous, layered $LiNi_{0.8}Co_{0.1}Mn_{0.1}O_2$ cathode materials were successfully synthesized via co-precipitation at optimum conditions, and the samples that were obtained exhibited a spherical morphology, high tap-density and high capacity. Furthermore, we could control the morphology of the precursor particles by adjusting the conditions during synthesis.

2) The particles size of the precursors was dependent on the process variables during co-precipitation. An increase in pH from 11.2 to 11.8, stirring speed from 500 to 800 rpm and residence time from 8 to 12 h resulted in a decrease in particle size while the increase in molar ratio of NH_4OH to metal from 0.8 to 1.2 and temperature from 45 to 55 °C did not have any consistent effect on the particle size. The optimum conditions for synthesis were thus determined according to these results.

3) All of the $LiNi_{0.8}Co_{0.1}Mn_{0.1}O_2$ samples obtained in this study exhibited clear XRD peak splits of 006/102 and 108/110 and a high c/a value, which indicates that the $LiNi_{0.8}Co_{0.1}Mn_{0.1}O_2$ materials have a well-ordered hexagonal structure.

4) The calcination temperature heavily influences the structure and the electrochemical performance of the samples. The results of the electrochemical experiments indicate that the layered $LiNi_{0.8}Co_{0.1}Mn_{0.1}O_2$ cathode materials that were calcined at 800 °C for 16 h possessed the highest initial discharge capacity of 193.7 mAh g^{-1} at a current density of 18.5 mAh g^{-1} in the voltage range from 3.0 to 4.3 V with a good rate capability.

5) The CV curves showed negligible differences in peak intensity and position in subsequent cycles after the 1st cycle, which indicates that the $LiNi_{0.8}Co_{0.1}Mn_{0.1}O_2$ samples have excellent stability during Li-ion intercalation and de-intercalation.

REFERENCES

1. A. Kraytsberg and Y. Ein-Eli, *Adv. Energy Mater.*, **2**, 922 (2012).
2. K. Zaghib, A. Mauger, H. Groult, J. Goodenough and C. Julien, *Materials (Basel)*, **6**, 1028 (2013).
3. B. L. Ellis, K. T. Lee and L. F. Nazar, *Chem. Mater.*, **3**, 691 (2010).
4. F. Liu, S. Song, D. Xue and H. Zhang, *Nanoscale Res. Lett.*, **7**, 149 (2012).
5. J. B. Goodenough and Y. Kim, *Chem. Mater.*, **22**, 587 (2010).
6. K. Mizushima, P. C. Jones, P. J. Wiseman and J. B. Goodenough, *Mater. Res. Bull.*, **15**, 783 (1980).
7. M. S. Whittingham, *Chem. Rev.*, **104**, 4271 (2004).
8. K. Ozawa, *Solid State Ionics*, **69**, 212 (1994).
9. Z. Wang, Z. Wang, H. Guo, W. Peng and X. Li, *Ceram. Int.*, **41**, 469 (2015).
10. G. Amatucci, *Solid State Ionics*, **83**, 167 (1996).
11. J. M. Tarascon and M. Armand, *Nature*, **414**, 359 (2001).
12. C. M. Julien, A. Mauger, K. Zaghib and H. Groult, *Inorganics*, **2**, 132 (2014).
13. P. Kalyani and N. Kalaiselvi, *Sci. Technol. Adv. Mater.*, **6**, 689 (2005).
14. Y.-K. Sun, Z. Chen, H.-L. Noh, D.-J. Lee, H.-G. Jung, Y. Ren, S. Wang, C. S. Yoon, S.-T. Myung and K. Amine, *Nat. Mater.*, **11**, 942 (2012).
15. D. P. Abraham, R. D. Twesten, M. Balasubramanian, I. Petrov, J. McBreen and K. Amine, *Electrochem. Commun.*, **4**, 620 (2002).
16. B. J. Hwang, Y. W. Tsai, D. Carlier and G. Ceder, *Chem. Mater.*, **15**, 3676 (2003).
17. S. Zhang, C. Deng, B. L. Fu, S. Y. Yang and L. Ma, *Powder Technol.*, **198**, 373 (2010).
18. J. J. Saavedra-Aria, N. K. Karan, D. K. Pradhan, A. Kumar, S. Nieto, R. Thomas and R. S. Katiyar, *J. Power Sources*, **183**, 761 (2008).
19. H. Lu, H. Zhou, A. M. Svensson, A. Fossdal, E. Shreidan, S. Lu and F. V. Bruer, *Solid State Ionics*, **249**, 105 (2013).
20. G. Ting-Kuo Fey, J.-G. Chen, Z.-F. Wang, H.-Z. Yang and T. P. Kumar, *Mater. Chem. Phys.*, **87**, 246 (2004).
21. G. T.-K. Fey, V. Subramanian and C.-Z. Lu, *Solid State Ionics*, **152-153**, 83 (2002).
22. G. T. K. Fey, R. F. Shiu, V. Subramanian, J. G. Chen and C. L. Chen, *J. Power Sources*, **103**, 265 (2002).
23. L. I. Ling-jun, L. I. Xin-hai, W. Zhi-xing, W. Ling, Z. Jun-chao and L. Jin-hui, *Trans. Nonferrous Met. Soc. China.*, **20**, 279 (2010).
24. Y. Zhang, H. Cao, J. Zhang and B. Xia, *Solid State Ionics*, **177**, 3303

(2006).
25. B. Zhang, L. Li and J. Zheng, *J. Alloys Compd.*, **520**, 190 (2012).
26. L.-J. Li, X.-H. Li, Z.-X. Wang, H.-J. Guo, P. Yue, W. Chen and L. Wu, *Powder Technol.*, **206**, 353 (2011).
27. J. J. Saavedra-Arias, C. V. Rao, J. Shojan, A. Manivannan, L. Torres, Y. Ishikawa and R. S. Katiyar, *J. Power Sources*, **211**, 12 (2012).
28. S. Choo, H. Y. Kim, D. Y. Yoon, W. Choi, S. H. Oh, J. B. Ju, J. M. Ko, H. Jang and W. I. Cho, *Korean J. Chem. Eng.*, **31**, 905 (2014).
29. K. Wu, F. Wang, L. Gao, M.-R. Li, L. Xiao, L. Zhao, S. Hu, X. Wang, Z. Xu and Q. Wu, *Electrochim. Acta*, **75**, 393 (2012).
30. I. Belharouak, W. Lu, D. Vissers, and K. Amine, *Electrochem. Commun.*, **8**, 329 (2006).
31. J. Ying, C. Wan, C. Jiang, and Y. Li, *J. Power Sources*, **99**, 78 (2001).
32. K. K. Cheralathan, N. Y. Kang, H. S. Park, Y. J. Lee, W. C. Choi, Y. S. Ko and Y. K. Park, *J. Power Sources*, **195**, 1486 (2010).
33. M.-H. Lee, Y.-J. Kang, S.-T. Myung and Y.-K. Sun, *Electrochim. Acta*, **50**, 939 (2004).
34. S. Zhang, C. Deng, B. L. Fu, S. Y. Yang and L. Ma, *Powder Technol.*, **198**, 373 (2010).
35. C. Fu, G. Li, D. Luo, Q. Li, J. Fan and L. Li, *ACS Appl. Mater. Interfaces*, **6**, 15822 (2014).
36. F. Lin, I. M. Markus, M. M. Doeff and H. L. Xin, *Sci. Rep.*, **4**, 5694 (2014).
37. D. Luo, G. Li, C. Fu, J. Zheng, J. Fan, Q. Li and L. Li, *J. Power Sources*, **276**, 238 (2015).
38. J.-T. Son and E. Cairns, *Korean J. Chem. Eng.*, **24**, 888 (2007).
39. O. Sekizawa, T. Hasegawa, N. Kitamura and Y. Idemoto, *J. Power Sources*, **196**, 6651 (2011).
40. J. Eom, M. G. Kim and J. Cho, *J. Electrochem. Soc.*, **155**, A239 (2008).
41. H. Bang, D.-H. Kim, Y. C. Bae, J. Prakash and Y.-K. Sun, *J. Electrochem. Soc.*, **155**, A952 (2008).
42. Y. Chen, Y. Zhang, B. Chen, Z. Wang and C. Lu, *J. Power Sources*, **256**, 20 (2014).
43. K. Liu, G.-L. Yang, Y. Dong, T. Shi and L. Chen, *J. Power Sources*, **281**, 370 (2014).
44. J. Zhao, S. Aziz and Y. Wang, *J. Power Sources*, **247**, 95 (2014).
45. K.-S. Lee, S.-T. Myung, K. Amine, H. Yashiro and Y.-K. Sun, *J. Electrochem. Soc.*, **154**, A971 (2007).